

1 **Supporting Online Material for**

2

3 **Anaerobic, nitrate-dependent oxidation of pyrite**

4 **nanoparticles by *Thiobacillus denitrificans***

5 Julian Bosch, Keun-Young Lee, Guntram Jordan, Kyoung-Woong Kim, Rainer U. Meckenstock

6

7

8

9 **This file includes 11 pages, 8 figures, and 4 tables on:**

10

11 Additional SEM-Pictures of the nanopyrite prior to incubation

12 Post-experimental SEM-pictures of nanopyrite

13 FeS positive control experiments

14 Reproduction of the main experiment with similar pyrite nanoparticles

15 Pyrite particle size information

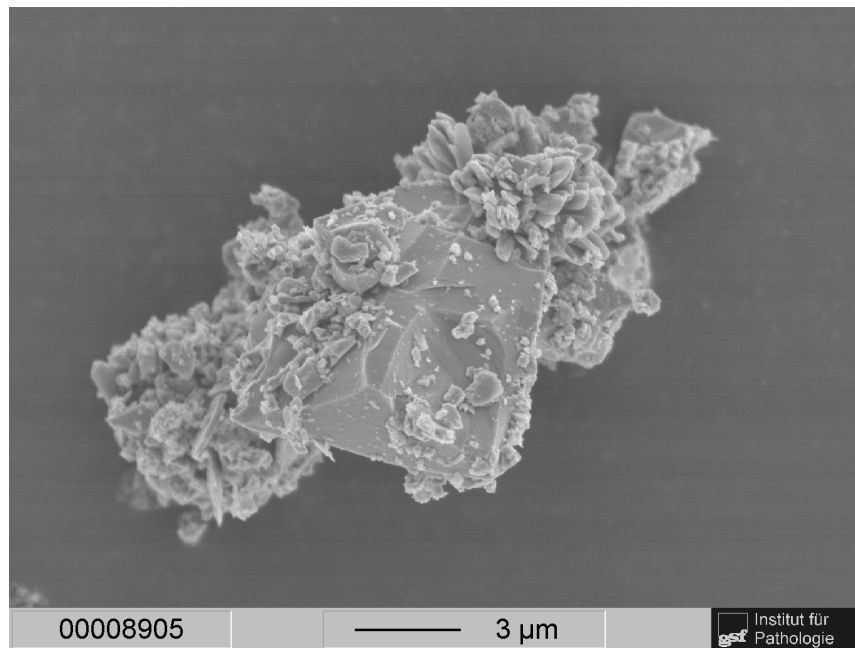
16 Experimental data overview table for main experiments

17 Trace elements analysis of pyrite

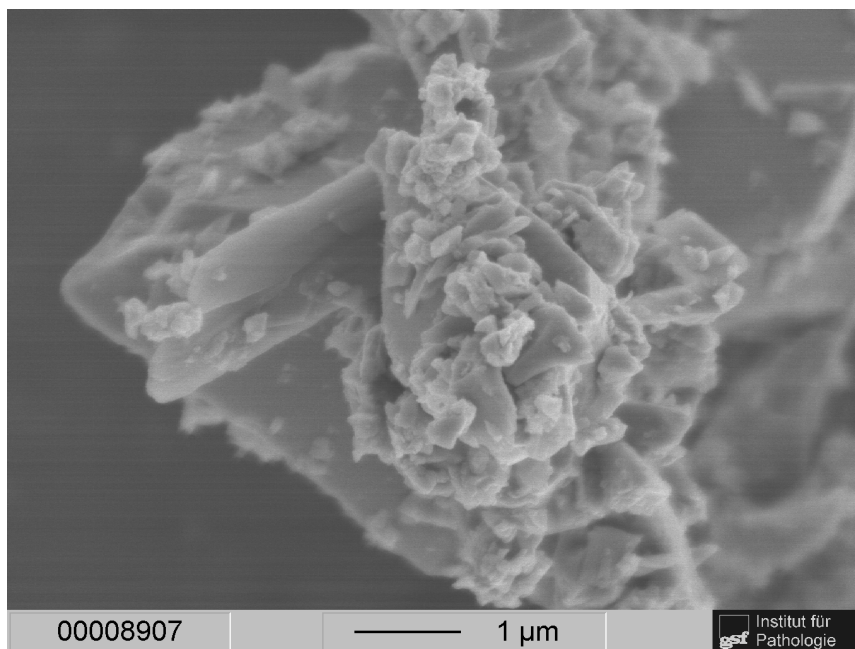
18 XRD detailed analysis

1 **Additional SEM-Pictures of the nanopyrite prior to incubation**

2
3



4
5



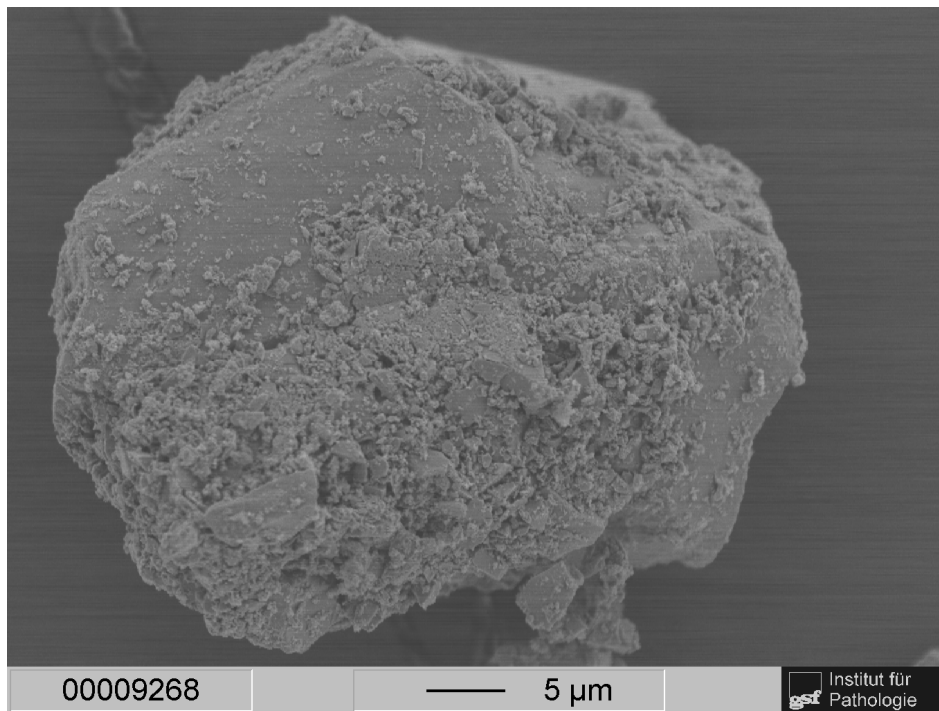
6
7

8 Fig. S1. SEM-Pictures of the applied micro- to nanosized pyrite at different magnifications. Apart
9 from the large, several-μm-crystals, there is a distinct nanoparticulate fraction of pyrite visible.

10

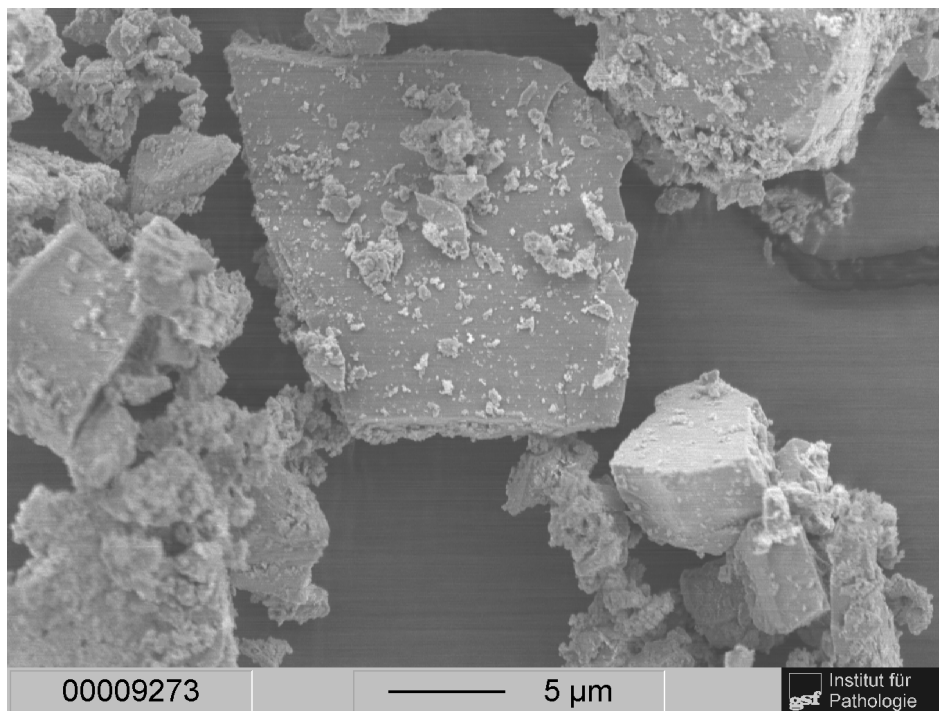
1 **Post-experimental SEM-pictures of nanopyrite**

2



3

4

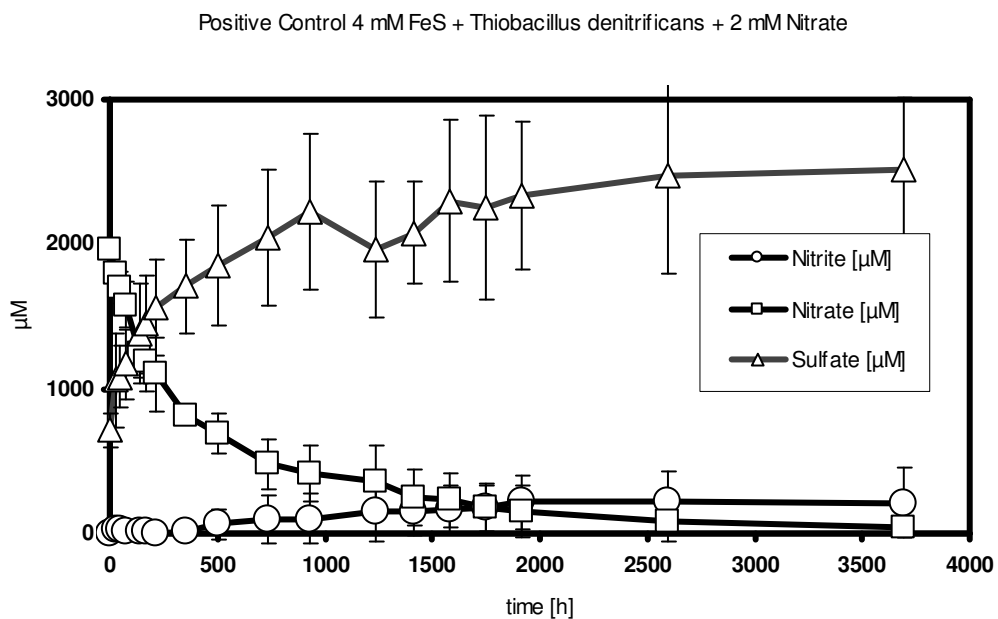


5

6 Fig. S2. SEM-Pictures of nanosized pyrite after the experiment. Large crystals remained
7 unaltered, while nanoparticles appear different from pre-experimental SEM-pictures. Same scale
8 as in Fig. S1 is not available.

1
2
3
4

FeS-control Experiments

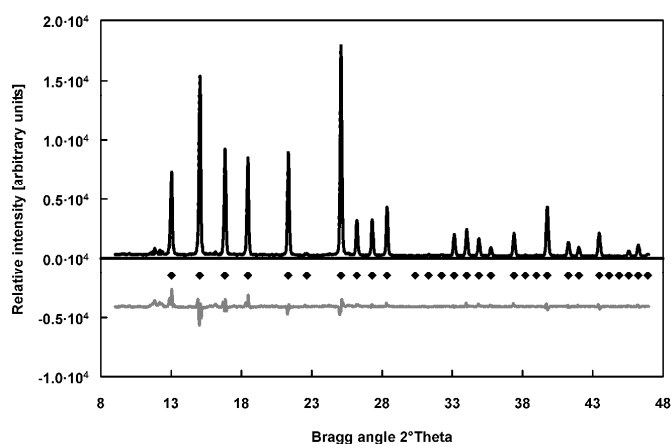


5
6
7
8
9
10
11

Fig. S3. Positive control. A dense suspension of *Thiobacillus denitrificans* was added to 4 mM FeS (Sigma) and 2 mM Nitrate in anoxic medium. Unlike the main experiments, a partial complete reduction of nitrate to nitrogen gas seems to occur with FeS as electron donor.

1
2 **Reproduction of the main experiment with similar pyrite nanoparticles**
3
4 A different preparation of pyrite was used similar to the pyrite used in the main manuscript. Due
5 to unidentified variations in the production, handling and storage of this material, a slight
6 contamination of a ferrous sulfate, probably szomolnokite was present in this material (Fig. S4).
7 This could be identified by weak XRD peaks at ~ 8-12 of 2°Theta Bragg angle defraction.
8 The experiment described therein was not a fully identical reproduction, as the ferrous sulfate had
9 an impact on the electron balance.
10 This material was added to dense, active cell suspensions of *Thiobacillus denitrificans* ($1.2 \cdot 10^6$
11 cells ml^{-1}) at a pyrite concentration of 2.1 mM as determined by total dissolution and
12 measurement by ICP-AES.

13

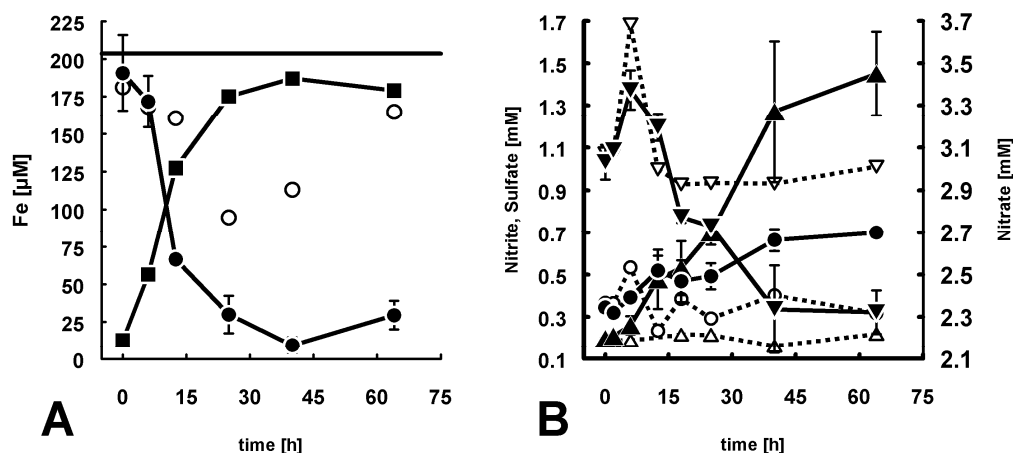


14

15 **Fig. S4.** XRD spectra of pyrite nanoparticles used for anaerobic
16 oxidation experiments. Obtained diffraction peaks (black line)
17 clearly occur at the theoretically expected positions (◆). Grey
18 line: quality of simulation.

19

1 Only ~10% out of this total pyrite were soluble in 1 M HCL, putatively the nanosized fraction
 2 (Fig. S5a). Nitrate was added as electron acceptor at 3 mM to the anoxic reaction medium.
 3 Within 40 h, pyrite nanoparticles were oxidized to Fe³⁺ and sulfate, at an initial maximum rate of
 4 6.4 μM h⁻¹, or 5.3 femtomol ferrous iron h⁻¹ per cell (Fig. S5a). Sterile controls did not show any
 5 reactions. An exception was an intermediate decrease in ferrous iron, which might be due to
 6 adsorption/desorption phenomena of the nanoparticulate pyrite fraction or recrystallization to
 7 larger crystals. Sulfate and nitrate concentration showed slight incongruities in terms of
 8 intermediate release and consumption. However, this stayed largely within measurement
 9 impreciseness.
 10
 11



12
 13
 14 **Fig. S5.** Anaerobic, nitrate-dependent oxidation of pyrite microparticles by *Thiobacillus denitrificans* over time. A:
 15 oxidation of pyrite Fe²⁺ (●) and formation of Fe³⁺ (■). Fe²⁺ in sterile control (○). Black line at 204 μM represents the
 16 fraction of total pyrite accessible by 1M HCL. B: Reduction of nitrate (▼) to nitrite (▲) and increase of sulfate (●)
 17 due to anaerobic pyrite oxidation. Sterile controls showed no reaction (respective open symbols and dashed lines).
 18 Error bars show standard deviations of three parallel incubations. Error bars of the sterile controls were omitted for
 19 clarity
 20

1 In our experiment, 0.16 ± 0.01 mM (89 %) of the acid-soluble pyrite fraction were oxidized to
 2 ferric iron and sulfate. The acid-insoluble fraction (~ 90 %) apparently remained unaltered by the
 3 microbial oxidation reaction, which was supported by SEM images.
 4 Based on the Fe^{2+} decrease within the acid-soluble pyrite fraction and concomitant SO_4^{2-}
 5 increase, 3.8 ± 0.2 mM of electrons from pyrite were delivered to nitrate by pyrite oxidation.
 6 Nitrate was reduced incomplete to nitrite instead of N_2 (Fig. S6b). This accounted for 2.3 ± 0.3
 7 mM e^- (according to eq. 2, main manuscript) and an electron recovery of 61 %. Additionally, the
 8 stoichiometry of the reaction showed an excess release of sulfate, which can be attributed to the
 9 share of szomolnokite in this particular pyrite preparation. Yet, the experimentally determined
 10 ratio of products to educts comes close to the expected theoretical ratio of the redox reaction
 11 products and educts (Tab. S1).

12
 13 **Tab. S1.** Mass balance of educts and products from anaerobic pyrite oxidation by *Thiobacillus*
 14 *denitrificans*. Ratio normalized to amount of depleted Fe^{2+} for pyrite nanoparticles and compared
 15 to ratio according to eq. 2.

	$\text{Fe}^{2+}/\text{Fe}^{3+}$ turnover [mM]	SO_4^{2-} produced [mM]	NO_2^- produced [mM]	NO_3^- depleted [mM]	Fe^{2+} ratio	SO_4^{2-} ratio	NO_2^- ratio	NO_3^- ratio
pyrite nanoparticles	0.16 ± 0.01	0.46 ± 0.07	1.33 ± 0.23	1.00 ± 0.16	1	2.9	8.5	6.4
theoretical ratio eq. (2)					1	2	7.5	7.5

17

18

19

20

21

22 **Pyrite Particle Size Information**

1
2 Particle size was measured by PCS as described in the main manuscript. The dominant peak (77
3 % peak weight) was the fraction of particles with a radius between 375 to 1317 nm (Table S2).
4 As can be seen from the data, the particle size distributions is broad, with an average size radius
5 of $1.2\pm 0.2 \mu\text{m}$.
6 Another peak (peak weight of 23%) was detected at sizes $> 13 \mu\text{m}$, which represents all large,
7 sedimenting particles on the edge of detection. Such particles cannot be assessed by PCS, so the
8 indication of 77 % refers only to particles in suspension.

9
10 **Tab. S2.** Size Distribution of the putatively
11 nanosized pyrite particle fraction

Peak 1	Mean	SD
from [nm]	375	89
to [nm]	1317	615
Weight of Peak [%]	77	6

12

1 **Experimental data overview table for main experiments**

2

3

Tab. S3. Overview of all relevant changes in the main manuscript experiment and its controls. Post-experimental cell density was not measured. All experiments were performed in triplicate, anoxically and in the dark.

6

	biotic	abiotic	no pyrite
organisms added:	<i>Thiobacillus</i>	-	<i>Thiobacillus</i>
electron donor:	nanopyrite	nanopyrite	-
electron acceptor:	nitrate	nitrate	nitrate
nitrate depleted [mM]	0.70 ± 0.04	0.08 ± 0.01	0.17 ± 0.08
sulfate produced [mM]	0.27 ± 0.02	0.00 ± 0.01	0.07 ± 0.06
nitrite produced [mM]	0.67 ± 0.04	0.00 ± 0.01	0.00 ± 0.01
ferrous iron to ferric iron [mM]	0.13 ± 0.02	0.00 ± 0.01	0.00 ± 0.01
pH change (initial: 6.8-7.2)	none	none	none

7

8

9

1 **Trace element analysis of pyrite**

2 The material used in the main experiments was analysed by ICP-AES (see main manuscript) to
3 check the presence of elements other than iron and sulfur. Only a few elements could be detected
4 at all (see Tab. S4). These elements were present only in the low per-mille of dry weight range,
5 excluding any effects of these elements on the reaction described in the main manuscript.

6

7

Tab. S4. Contents of elements other
8 than iron and sulfur in the pyrite
9 material applied in the main
10 manuscript experiments.

9

10

<u>Element</u>	<u>[%] of dry weight</u>
Co	0,004
Cu	0,042
Mn	0,003
Mo	0,004
Ni	0,004
Pb	0,106
Sb	0,007
Zn	0,145

11

XRD - detailed analysis of small peaks

During the XRD results evaluation, we observed that pyrite preparation contaminations like e.g. ferrous sulfates could typically be observed in the low 2°Theta range between 8 and 12. We want to emphasize that our nanoparticulate pyrite preparation, which was applied to the experiments of the main manuscript, contained no such contaminations. Therefore, we present a detailed picture of Fig. 1 of the main manuscript (Fig. S6). Clearly, no phases related to iron or sulfur other than pyrite are present in our pyrite preparation. In comparison, the material used for the reproduction contained $\sim 8\%$ of szomolnokite, indicated by a peak at $\sim 11.1^\circ\text{Theta}$.

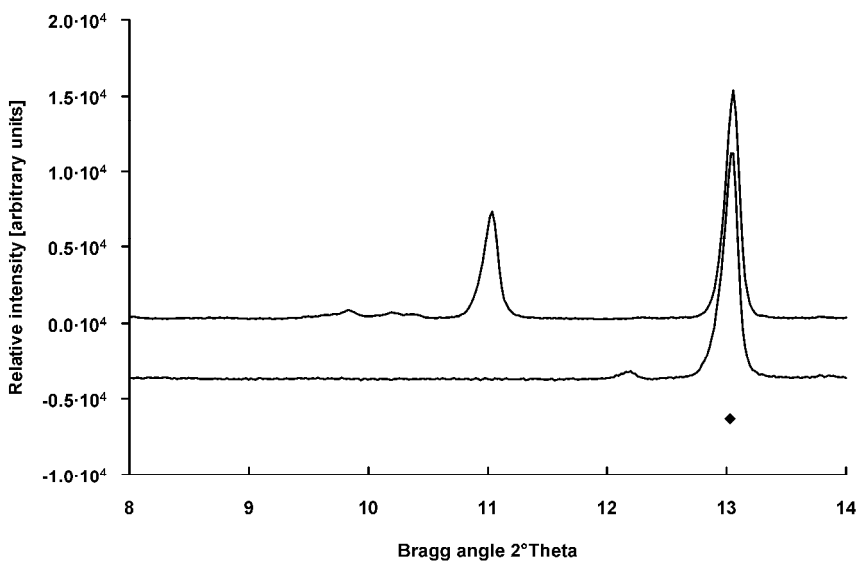


Fig. S6. XRD pattern of the two pyrite preparations used in this publication. Upper graph: pyrite from the reproduction experiment. Lower Graph: pyrite used in the main manuscript.

The reference peak for pyrite at 13.1°Theta is marked with a symbol (◆).